NEURAL NETWORKS AS A MEANS TO FIT THE POTENTIAL ENERGY SURFACE OF VINYL BROMIDE

By

DANY IBRAHIM DOUGHAN

Bachelor of Science
Lebanese American University
Beirut, Lebanon
1998

Master of Science
Lebanese American University
Beirut, Lebanon
2001

Submitted to the Faculty of the
Graduate College of the
Oklahoma State University
in partial fulfillment of
the requirements for
the Degree of
MASTER OF SCIENCE
May, 2004

NEURAL NETWORKS AS A MEANS TO FIT THE

POTENTIAL ENERGY SURFACE

OF VINYL BROMIDE

Thesis Approved:

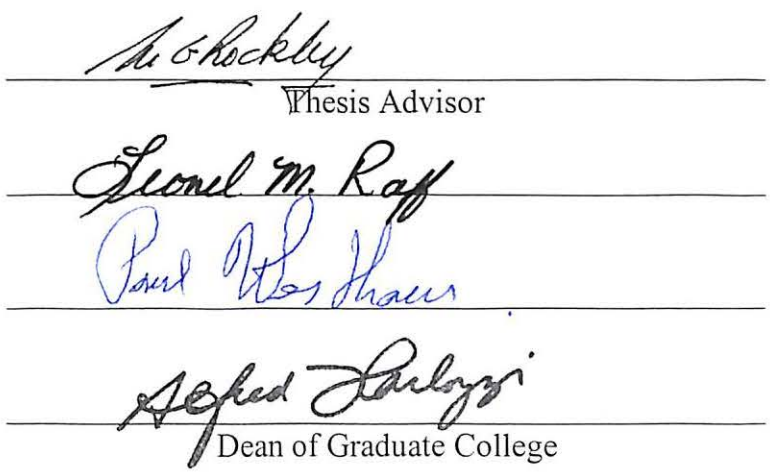

Thesis Advisor

Dean of Graduate College

ACKNOWLEDGEMENTS

I wish to express my sincere appreciation to my research advisors, Dr. Lionel Raff and Dr. Mark Rockley for their guidance, patience and inspiration during my research work.

I would also like to thank Dr. Paul Westhaus for serving on my committee and taking the time to read this thesis.

Moreover, I wish to express my sincere gratitude to my friends for their warm friendship, discussion and suggestions.

I would also like to give my special appreciation to my parents, my fiancée and family members for their support and encouragement for all the time.

Finally, I would like to thank the Department of Chemistry for supporting me during my studies.

TABLE OF CONTENTS

LIST OF TABLES

LIST OF FIGURES

Figure Page

CHAPTER I

INTRODUCTION

In order to investigate the reaction dynamics and spectroscopy of molecular systems, knowledge of the potential-energy surface (PES) is needed. For molecules that are made up of more than three atoms, the accurate calculation of the PES is very difficult because of the dimensionality of the surface. A large dimensionality makes it very difficult to obtain high-level electronic structure calculations for a sufficiently large number of configurations to be able to obtain a global characterization of the PES.

The level of difficulty associated with obtaining a global PES has led to several attempts to predict reaction mechanisms by using the relative energies of stationary-points, maxima and minima on the surface, without having to explore the whole PES.[1,2] The number of stationary-points is small which means that their energies can be calculated accurately at the fourth-order Möller-Plesset perturbation (MP4) level or higher with large basis sets.[3-5]

By assuming that reactions follow the minimum-energy path, reaction mechanisms can be inferred from the knowledge of stationary-point energies.[6-16] For thermal decompositions, this assumption is quite accurate. This technique yields accurate results provided that the reactions occur at energies fairly close to the potential barrier.

Another approach employed to characterize the global PES is to use parameterized functional forms justified chemically and physically to fit the thermochemical, spectroscopic, structural and kinetic data.[17-23] This technique usually yields results that are semiquantitatively accurate as long as the critical potential barriers of reactions are accurately estimated from measured activation energies.[24,25]

The most successful approach employed to date to obtain a reasonably accurate PES is a combination of the above methods.[26] In this method, high-level *ab initio* calculations are performed to obtain transition-state geometries, frequencies and energies, which are then fitted using ad hoc empirical functional forms. [27-30] Although the empirical function may have more than one hundred adjustable parameters, this is usually insufficient to fit all the *ab initio* and experimental data. This is why, whenever a PES is developed for a polyatomic system, the computed results are open to criticism related to the reliability of the surface. Clearly, a more efficient method is needed.

We intend to carry out sensitivity studies that allow us to determine important topographical features of the PES such as reaction pathways, product yields and ratios, intramolecular vibrational energy relaxation (IVR) rates and reaction rates in an efficient and reliable manner. To achieve this goal we will be carefully sampling the potential hypersurface and fitting it with a neural network.

We shall study the gas-phase decomposition reaction of vinyl bromide, a system that is sufficiently large to represent a polyatomic system but not so large as to render the computations intractable. This system has been studied both experimentally and theoretically, which means that enough *ab initio* and experimental data are available to

allow for a careful evaluation of the accuracy of the surface and the predicted dynamics that we obtain in our investigations.

The thermal and photolytic unimolecular decomposition reactions of vinyl bromide and the reverse bimolecular reaction of HBr with acetylene in the gas phase have been studied experimentally and theoretically. Using shock tube methods, Saito *et al.* investigated the gas-phase decomposition of vinyl bromide between 1300 K and 2000 K.[31-33] It was reported that the reaction proceeds solely via elimination of HBr according to the following reaction:

$$H_2C{=}CHBr \rightarrow HBr + HC{\equiv}CH$$

However, it was not known whether the HBr elimination occurs via a three-center or a four-center elimination reaction.

The two possible reactions are the following:

$$H_2C{=}CHBr \rightarrow HBr + HC{\equiv}CH$$

$$H_2C{=}CHBr \rightarrow HBr + H_2C{=}C \rightarrow HBr + HC{\equiv}CH$$

Wodtke *et al.*[34] have photolyzed a molecular beam of vinyl bromide at 193 nm and product fragments were determined using mass analysis. Their results indicate that the predominant reaction is not molecular HBr elimination but rather Br atom dissociation according to the following reaction because the reaction occurs on an electronically-excited potential surface:

$$H_2C{=}CHBr \rightarrow Br + C_2H_3$$

Johnston and Price[35], using xenon-filled lamps that emit between 150 nm and 200 nm, reported that HBr, not Br, is the main product of the reaction. Neither Johnston and Price[35] nor Wodtke *et al.*[34] detected any formation of molecular H or bromoacetylene.

Photolysis experiments under matrix-isolated conditions reported by Abrash *et al.*[36,37] showed that the only primary products are HBr and acetylene formed in either a three-center or a four-center elimination. The results showed no Br atom formation but an important secondary channel leading to H_2 and bromoacetylene is observed. The reaction channel is the following:

$$H_2C{=}CHBr \rightarrow H_2 + HC{\equiv}CBr$$

A possible mechanism, which might explain these results, is the dissociation of HBr followed by cage recombination to form excited HBr that adds to acetylene in order to give C_2HBr and H_2.

Ebert *et al.*[38] investigated the gas-phase collision between HBr and acetylene and found that hydrogen exchange is the main reaction channel when both HBr and acetylene are in their vibrational ground states.

Abrash *et al.*[39] reported classical trajectory studies of the gas-phase decomposition of vinyl bromide using a ground state, empirical potential-energy surface. The dissociation dynamics were studied between 4.00 eV and 6.44 eV and showed that the decomposition dynamics follow a first-order rate law. At E = 6.44 eV, the reaction channels are, in order of importance, H_2 elimination, HBr elimination, Br atom dissociation and C-H bond fission.

Mains *et al.*[40] studied the decomposition of vinyl bromide upon single-photon excitation at 193 nm using classical trajectory methods on an adiabatic excited-state PES. Their studies indicate that the only products are the vinyl radical and Br meaning that the *ab initio* excited stated are repulsive.

Rahaman and Raff[41,42] investigated the reaction dynamics of vibrationally excited vinyl bromide using classical trajectory methods on a global, analytic potential-energy hypersurface. The calculations were carried out at the MP4 level of theory and focus on the determination of the dependence of the potential upon the stretching of the coordinates for the bonded atoms in vinyl bromide, the C-C-H and C-C-Br bending coordinates and the dihedral angles.

The PES fitted to the total *ab initio* calculations data base is then modified by adjustment of the potential curvatures at equilibrium to provide a better fit to the measured IR and Raman vibrational frequencies of vinyl bromide while simultaneously holding all other topographical features of the surface constant to the maximum extent possible. The fitting process took over 9 months to be completed because as one part of the hypersurface was fitted another part of the surface would be affected, which needed to be fitted, so on and so forth. This iterative process was the most time consuming one. The dissociation dynamics were investigated between 4.50 eV and 6.44 eV.

The results indicate that small variations in potential-energy curvatures at equilibrium and along the reaction coordinates do not exert significant influence upon the dissociation dynamics. The computed results for the HBr vibrational energy distributions were in excellent accord with experimental measurements.

References:

1. N. Bakkas, T. Bouteiller, Aloutellier, J. P. Perchard and S. Racine, *J. Chem. Phys.* **99**, 3335 (1993).

2. B. D. Waldowski, A. L. L. East, J. E. Mihalick W. D. Allen and J. I, Braumann, *J. Chem. Phys.* **100**, 2058 (1994).

3. S. P. Walch, *J. Chem. Phys.* **98**, 3163 (1993).

4. S. P. Walch, *J. Chem. Phys.* **99**, 5295 (1993).

5. S. H. Robertson, D. M. Wardlaw and D. M. Hirst, *J. Chem. Phys.* **99**, 7748 (1993).

6. A.M. Mebel, K. Morokuma and M. C. Lin, *J. Chem. Phys.* **101**, 3916 (1994).

7. S. A. Maluendes, A. D. McLean, K. Yamashita and E. Herbst *J. Chem. Phys.* **99**, 2812 (1993).

8. T. H. Dunning, *J. Chem. Phys.* **55**, 716 (1971).

9. S. Huzinaga, *J. Chem. Phys.* **42**, 1293 (1965).

10. J. H. Jensen, K. Morokuma and M. S. Gordon, *J. Chem. Phys.* **100**, 1981 (1994).

11. H. Okabe and J. R. McNesby, *J. Chem. Phys.* **36**, 601 (1992).

12. B. A. Balko, J. Zhang and Y. T. Lee, *J. Chem. Phys.* **97**, 935 (1992).

13. J. F. Riehl and K. Morokuma *J. Chem. Phys.* **100**, 8976 (1994).

14. P. Ausloos, R. E. Rebbert and M. H. Wijnen, *J. Res. Nat. Bur. Std.* **77a**, 243 (1973).

15. C. Reiser, F. M. Lussier, C. C. Jensen and J. I. Steinfeld, *J. Am. Chem. Soc.* **101**, 350 (1979).

16. Y. Huang, Y. Yang, G. He and R. J. Gordon. *J. Chem. Phys.* **99**, 2752 (1993).

17. T. D. Swell and D. L. Thompson, *J. Chem. Phys.* **93**, 4077 (1990).

18. A. J. Marks, *J. Chem. Phys.* **100**, 8096 (1994).

19. B. M. Rice and D. L. Thompson, *J. Chem. Phys.* **93**, 7986 (1990).

20. R. Alimi, V. A. Apkarian and R. B. Gerber, *J. Chem. Phys.* **98**, 331 (1993).

21. G. Lendvay and G. C. Schatz, *J. Chem. Phys.* **96**, 4356 (1992).

22. G. Lendvay and G. C. Schatz, *J. Chem. Phys.* **98**, 1034 (1993).

23. F. E. Budenholzer, M. Y. Chang and K. C. Huang, *J. Chem. Phys.* **98**, 12501 (1994).

24. L. M. Raff, *J. Phys. Chem.* **91**, 3266 (1987).

25. L. M. Raff, *J. Phys. Chem.* **92**, 141 (1988).

26. L. M. Raff and R. W. Graham, *J. Phys. Chem.* **92**, 5111 (1988).

27. Y. J. Cho, S. R. Vande Linde, L. Zhu and W. L. Hase, *J. Chem. Phys.* **96**, 7962 (1990).

28. S. R. Vande Linde and W. L. Hase, *J. Chem. Phys.* **93**, 7962 (1990).

29. S. R. Vande Linde and W. L. Hase, *J. Chem. Phys.* **94**, 6148 (1990).

30. W. L. Hase and Y. J. Cho, *J. Chem. Phys.* **98**, 8626 (1993).

31. K. Saito, T. Yokubo, T. Fuse, H. Tahara, O. Kondo, T. Higashihara and I. Murakami, *Bull. Chem. Soc. Jpn.* **52**, 3507 (1979).

32. R. Krishnan, M. J. Frisch, J. A. Pople and P. V. R. Schleyer, *Chem. Phys. Lett.* **79**, 408 (1981).

33. (a) Y. Osamura, H. F., I. Schaefer, S. K. Gray and W. H. Miller, *J. Am. Chem. Soc.* **103**, 1904 (1981).

(b) B. J. Smith, R. Smernik and L. Radom, *Chem. Phys. Lett.* **188**, 589 (1992).

(c) Ph. Halvick, D. Liotard and J. C. Rayez, *Chem. Phys.* **177**, 69 (1993).

34. (a) A. M. Wodtke, E. J. Hintsa, J. Somorjai and Y. T. Lee, *Isr. J. Chem.* **29**, 383 (1989).

(b) A. M. Wodtke and Y. T. Lee, *J. Phys. Chem.* **89**, 4744 (1985).

35. G. R. Johnston and D. Price, *Dyn. Mass Spectrom.* **3**, 183 (1973).

36. S. A. Abrash Ph. D. Dissertation, University of California at Berkeley (1987).

37. S. A. Abrash, M. T. McMahon and R. W. Zehner, *J. Phys. Chem.* **98**, 11909 (1994).

38. M. E. Ebert, S. A. Abrash and L. M. Raff, *J. Phys. Chem.* **99**, 17691 (1995).

39. S. A. Abrash, R. W. Zehner, G. J Mains and L. M. Raff, *J. Phys. Chem.* **99**, 2959 (1995),

40. G. J. Mains, L. M. Raff and S. A. Abrash, *J. Phys. Chem.* **99**, 3532 (1995).

41. A. Rahaman Ph. D. Dissertation, Oklahoma State University at Stillwater (2000).

42. A. Rahaman and L. M. Raff, *J. Phys. Chem. A* **105**, 2156 (2001).

CHAPTER II

COMPUTATIONAL METHODS FOR OBTAINING AN AB INITIO POTENTIAL-ENERGY SURFACE

A. *Ab initio* Calculations

In order to obtain an accurate global potential-energy surface, it is important to know exactly how the potential varies due to stretching the bonds, bending the angles and twisting the dihedral angles. This requires high-level *ab initio* calculations for a large number of configurations.

We have carried out a series of *ab initio* calculations at the MP4(SDQ) level of theory using the GAUSSIAN 98W[1] package. For C and H atoms, we have used 6-31G(d,p) basis sets. Huzinaga's (4333/433/4) basis sets[2] augmented with split outer s and p orbitals (43321/4321/4) are used for the Br atom to improve the flexibility of the Br electron density. We also added a polarization f orbital with an exponent of 0.5 for a more accurate description of the Br atom.

The average computational time for an *ab initio* calculation on a 1.87 GHz AMD Athlon™ XP 2100+ was 57 seconds.

The way the atoms in the molecule of vinyl bromide were assigned is shown in Figure 2.1.

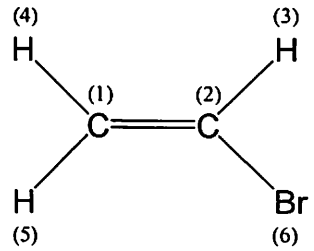

Figure 2.1

Atom assignment in vinyl bromide

We have performed a relaxed potential energy scan for all bonds, angles and dihedral angles. Each bond was stretched or compressed in increments of 0.1 Å from its equilibrium value for a reasonable length. The values of the different bond distances, angles and dihedral angles in the most stable configuration of vinyl bromide, with an MP4(SDQ) equilibrium potential energy of -2647.89414 Hartrees, are shown in Table 2.1.

Table 2.1

Equilibrium configuration of vinyl bromide

Z-matrix Coordinate		GAUSSIAN 98W[1] Values	Experimental Values[3,4]
$C^{(1)}=C^{(2)}$	bond distance	1.3364 Å	1.330 Å
$C^{(2)}$-$H^{(3)}$	bond distance	1.0799 Å	1.077 Å
$C^{(1)}$-$H^{(4)}$	bond distance	1.0830 Å	1.083 Å
$C^{(1)}$-$H^{(5)}$	bond distance	1.0816 Å	1.085 Å
$C^{(2)}$-$Br^{(6)}$	bond distance	1.9268 Å	1.890 Å
$C^{(1)}C^{(2)}H^{(3)}$	angle	124.1297 °	124.2 °
$C^{(2)}C^{(1)}H^{(4)}$	angle	119.6742 °	118.7 °
$C^{(2)}C^{(1)}H^{(5)}$	angle	122.2679 °	121.3 °
$C^{(1)}C^{(2)}Br^{(6)}$	angle	123.5391 °	122.5 °
$H^{(4)}H^{(3)}$	dihedral angle	-0.0088 °	0.0 °
$H^{(5)}H^{(3)}$	dihedral angle	-180.0047 °	180.0 °
$H^{(4)}Br^{(6)}$	dihedral angle	179.9962 °	180.0 °

At each increment, the energy of the molecule is calculated. Using this technique we were able to scan the potential for all bonds one at a time and obtain a potential curve with respect to each coordinate of the Z-matrix. 130 of the 600 *ab initio* potential energies "K" are shown in Tables 2.2 through 2.6. The relative *ab initio* potential energy "K_{Rel}" was calculated using the following formula where "K_{max}" refers to the maximum energy in the potential-energy curve and "K_{min}" refers to the minimum energy:

$$K_{Rel} = \frac{2\,(K - K_{min})}{K_{max} - K} - 1$$

Using this formula, we made sure that all the calculated relative values would fall between the values –1 and +1. The reason behind using this scaling will be discussed in a future section.

Table 2.2

Ab initio potential energy at different $C^{(1)}=C^{(2)}$ bond distances

$C^{(1)}=C^{(2)}$ Bond distance (Å)	*Ab initio* potential energy (Hartrees)	Relative a*b initio* potential energy
1.0364	-2647.71040	-0.33289
1.1364	-2647.82952	-0.76539
1.2364	-2647.88175	-0.95502
1.3364	-2647.89414	-1.00000
1.4364	-2647.88343	-0.96110
1.5364	-2647.86001	-0.87609
1.6364	-2647.83035	-0.76839
1.7364	-2647.79840	-0.65240
1.8364	-2647.76654	-0.53671
1.9364	-2647.73608	-0.42611
2.0364	-2647.70748	-0.32227
2.1364	-2647.67915	-0.21942

Table 2.3

Ab initio potential energy at different $C^{(2)}$-$H^{(3)}$ bond distances

$C^{(2)}$-$H^{(3)}$ Bond distance (Å)	*Ab initio* potential energy (Hartrees)	Relative a*b initio* potential energy
0.7799	-2647.77704	-0.57485
0.8799	-2647.85298	-0.85055
0.9799	-2647.88596	-0.97031
1.0799	-2647.89414	-1.00000
1.1799	-2647.88824	-0.97858
1.2799	-2647.87468	-0.92934
1.3799	-2647.85730	-0.86622
1.4799	-2647.83850	-0.79797
1.5799	-2647.81943	-0.72876
1.6799	-2647.80123	-0.66266
1.7799	-2647.78430	-0.60119
1.8799	-2647.76891	-0.54532

Table 2.4

Ab initio potential energy at different $C^{(1)}$-$H^{(4)}$ bond distances

$C^{(1)}$-$H^{(4)}$ Bond distance (Å)	*Ab initio* potential energy (Hartrees)	Relative a*b initio* potential energy
0.7830	-2647.77933	-0.58317
0.8830	-2647.85375	-0.85334
0.9830	-2647.88610	-0.97081
1.0830	-2647.89414	-1.00000
1.1830	-2647.88835	-0.97897
1.2830	-2647.87498	-0.93044
1.3830	-2647.85780	-0.86804
1.4830	-2647.83906	-0.80000
1.5830	-2647.82015	-0.73135
1.6830	-2647.80193	-0.66519
1.7830	-2647.78489	-0.60333
1.8830	-2647.76931	-0.54678

Table 2.5

Ab initio potential energy at different $C^{(1)}$-$H^{(5)}$ bond distances

$C^{(1)}$-$H^{(5)}$ Bond distance (Å)	*Ab initio* potential energy (Hartrees)	Relative a*b initio* potential energy
0.7816	-2647.77832	-0.57947
0.8816	-2647.85337	-0.85199
0.9816	-2647.88602	-0.97053
1.0816	-2647.89414	-1.00000
1.1816	-2647.88829	-0.97876
1.2816	-2647.87478	-0.92971
1.3816	-2647.85739	-0.86658
1.4816	-2647.83841	-0.79767
1.5816	-2647.81924	-0.72807
1.6816	-2647.80074	-0.66090
1.7816	-2647.78343	-0.59804
1.8816	-2647.76759	-0.54051

Table 2.6

Ab initio potential energy at different $C^{(2)}$-$Br^{(6)}$ bond distances

$C^{(2)}$-$Br^{(6)}$ Bond distance (Å)	*Ab initio* potential energy (Hartrees)	Relative a*b initio* potential energy
1.6268	-2647.84602	-0.82527
1.7268	-2647.87635	-0.93543
1.8268	-2647.89051	-0.98682
1.9268	-2647.89414	-1.00000
2.0268	-2647.89099	-0.98856
2.1268	-2647.88357	-0.96164
2.2268	-2647.87361	-0.92547
2.3268	-2647.86229	-0.88437
2.4268	-2647.85044	-0.84133
2.5268	-2647.83861	-0.79839
2.6268	-2647.82719	-0.75692
2.7268	-2647.81642	-0.71780

In a similar manner, each angle is varied from its equilibrium value in increments of 2° and at each increment, the potential energy of the molecule is calculated yielding the bending potential. A subset of the results is shown in Tables 2.7 through 2.10.

Table 2.7

Ab initio potential energy at different $C^{(1)}C^{(2)}H^{(3)}$ angles

$C^{(1)}C^{(2)}H^{(3)}$ Angle (°)	*Ab initio* potential energy (Hartrees)	Relative a*b initio* potential energy
118.1297	-2647.89282	-0.99519
120.1297	-2647.89356	-0.99788
122.1297	-2647.89400	-0.99948
124.1297	-2647.89414	-1.00000
126.1297	-2647.89398	-0.99943
128.1297	-2647.89352	-0.99776
130.1297	-2647.89276	-0.99498
132.1297	-2647.89168	-0.99108
134.1297	-2647.89030	-0.98604
136.1297	-2647.88859	-0.97985

Table 2.8

Ab initio potential energy at different $C^{(2)}C^{(1)}H^{(4)}$ angles

$C^{(2)}C^{(1)}H^{(4)}$ Angle (°)	*Ab initio* potential energy (Hartrees)	Relative a*b initio* potential energy
113.6742	-2647.89289	-0.99545
115.6742	-2647.89358	-0.99797
117.6742	-2647.89400	-0.99949
119.6742	-2647.89414	-1.00000
121.6742	-2647.89400	-0.99951
123.6742	-2647.89360	-0.99803
125.6742	-2647.89291	-0.99555
127.6742	-2647.89196	-0.99209
129.6742	-2647.89074	-0.98764
131.6742	-2647.88924	-0.98222

Table 2.9

Ab initio potential energy at different $C^{(2)}C^{(1)}H^{(5)}$ angles

$C^{(2)}C^{(1)}H^{(5)}$ Angle (°)	*Ab initio* potential energy (Hartrees)	Relative a*b initio* potential energy
116.2679	-2647.89285	-0.99530
118.2679	-2647.89357	-0.99791
120.2679	-2647.89400	-0.99947
122.2679	-2647.89414	-1.00000
124.2679	-2647.89401	-0.99951
126.2679	-2647.89358	-0.99797
128.2679	-2647.89288	-0.99543
130.2679	-2647.89191	-0.99189
132.2679	-2647.89066	-0.98736
134.2679	-2647.88914	-0.98183

Table 2.10

Ab initio potential energy at different $C^{(1)}C^{(2)}Br^{(6)}$ angles

$C^{(1)}C^{(2)}Br^{(6)}$ Angle (°)	*Ab initio* potential energy (Hartrees)	Relative a*b initio* potential energy
117.5391	-2647.89236	-0.99354
119.5391	-2647.89336	-0.99717
121.5391	-2647.89395	-0.99931
123.5391	-2647.89414	-1.00000
125.5391	-2647.89395	-0.99931
127.5391	-2647.89337	-0.99720
129.5391	-2647.89242	-0.99376
131.5391	-2647.89109	-0.98893
133.5391	-2647.88937	-0.98268
135.5391	-2647.88728	-0.97509

We performed the same potential energy scan for the dihedral angles of the vinyl bromide molecule in the same manner we performed it for the angles. A subset of the results is shown in Tables 2.11 through 2.13.

Table 2.11

Ab initio potential energy at different $H^{(4)}H^{(3)}$ dihedral angles

$H^{(4)}H^{(3)}$ Dihedral angle (°)	*Ab initio* potential energy (Hartrees)	Relative a*b initio* potential energy
-6.0088	-2647.89376	-0.99862
-4.0088	-2647.89397	-0.99938
-2.0088	-2647.89410	-0.99985
-0.0088	-2647.89414	-1.00000
1.9912	-2647.89410	-0.99985
3.9912	-2647.89397	-0.99938
5.9912	-2647.89377	-0.99866
7.9912	-2647.89347	-0.99757
9.9912	-2647.89309	-0.99619
11.9912	-2647.89262	-0.99448

Table 2.12

Ab initio potential energy at different $H^{(5)}H^{(3)}$ dihedral angles

$H^{(5)}H^{(3)}$ Dihedral angle (°)	*Ab initio* potential energy (Hartrees)	Relative a*b initio* potential energy
-186.0047	-2647.89376	-0.99862
-184.0047	-2647.89397	-0.99938
-182.0047	-2647.89410	-0.99985
-180.0047	-2647.89414	-1.00000
-178.0047	-2647.89410	-0.99985
-176.0047	-2647.89397	-0.99938
-174.0047	-2647.89376	-0.99862
-172.0047	-2647.89346	-0.99753
-170.0047	-2647.89307	-0.99612
-168.0047	-2647.89260	-0.99441

Table 2.13

Ab initio potential energy at different $H^{(4)}Br^{(6)}$ dihedral angles

$H^{(4)}Br^{(6)}$ Dihedral angle (°)	*Ab initio* potential energy (Hartrees)	Relative a*b initio* potential energy
173.9962	-2647.89370	-0.99840
175.9962	-2647.89394	-0.99927
177.9962	-2647.89409	-0.99982
179.9962	-2647.89414	-1.00000
181.9962	-2647.89409	-0.99982
183.9962	-2647.89394	-0.99927
185.9962	-2647.89370	-0.99840
187.9962	-2647.89335	-0.99713
189.9962	-2647.89291	-0.99553
191.9962	-2647.89236	-0.99354

In order to visualize the superset of the data found in Tables 2.2 through 2.13, we present them graphically in Figures 2.2 through 2.13 where the potential energy is calculated in units of eV with GAUSSIAN 98W[1] at the MP4(SDQ) perturbation level of theory. In Figures 2.2 through 2.13, the *ab initio* calculated potentials have been connected through lines for visual clarity only.

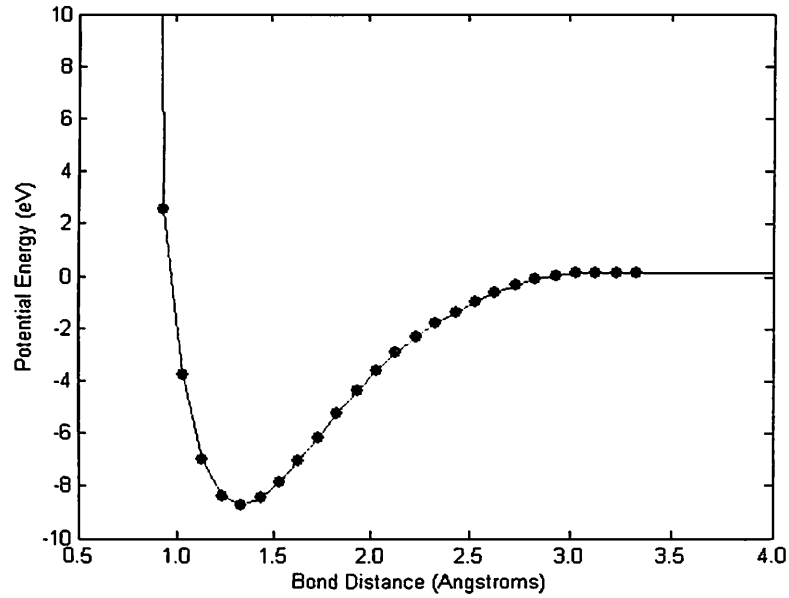

Figure 2.2

Ab initio potential energy at different $C^{(1)}=C^{(2)}$ bond distances

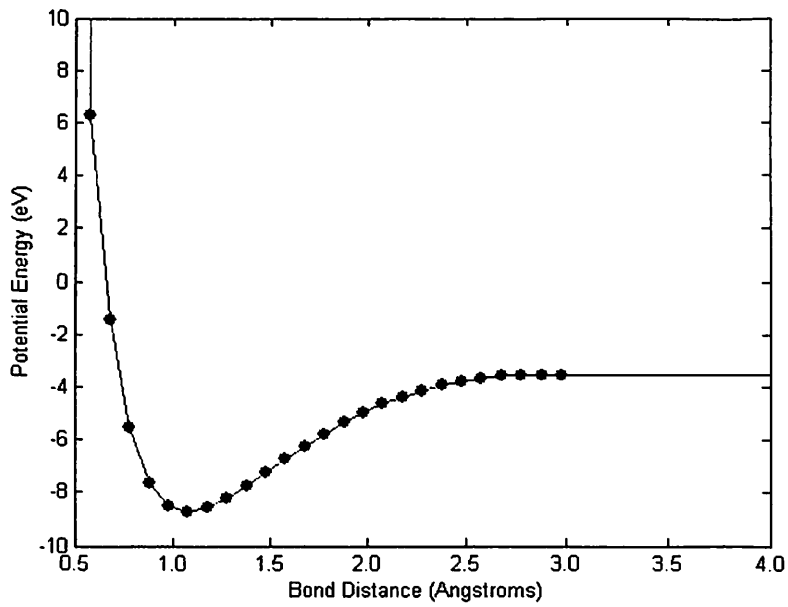

Figure 2.3

Ab initio potential energy at different $C^{(2)}$-$H^{(3)}$ bond distances

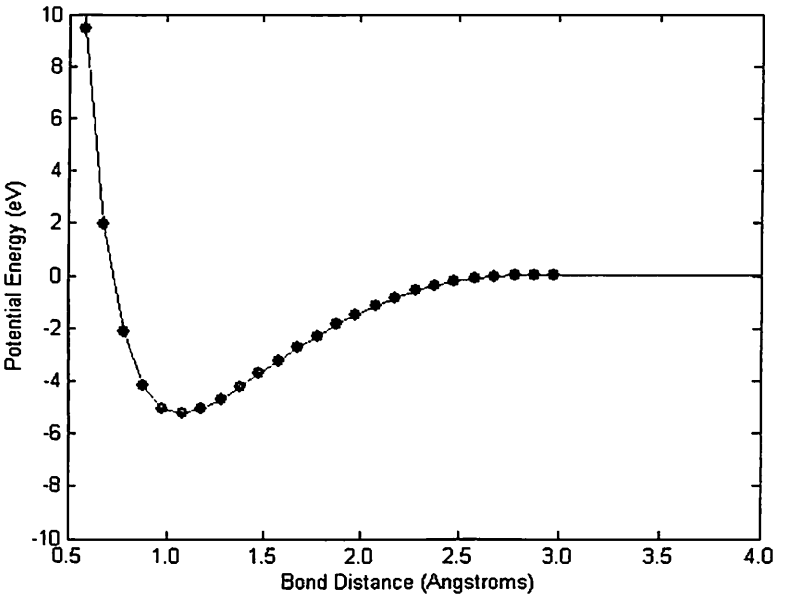

Figure 2.4

Ab initio potential energy at different $C^{(1)}$-$H^{(4)}$ bond distances

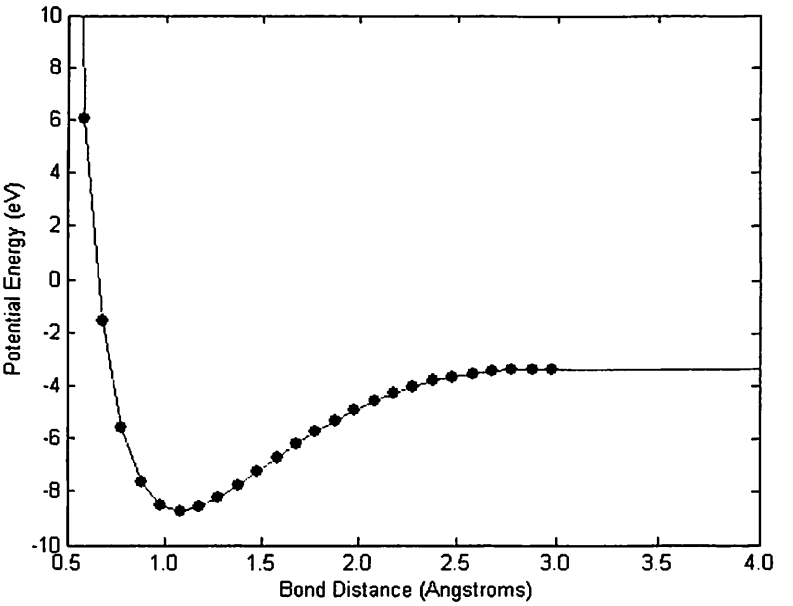

Figure 2.5

Ab initio potential energy at different $C^{(1)}$-$H^{(5)}$ bond distances

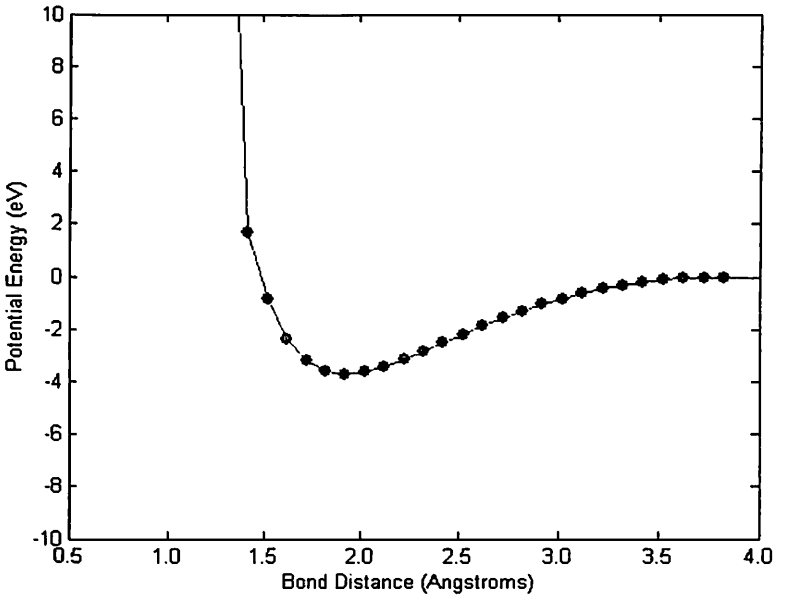

Figure 2.6

Ab initio potential energy at different $C^{(2)}$-$Br^{(6)}$ bond distances

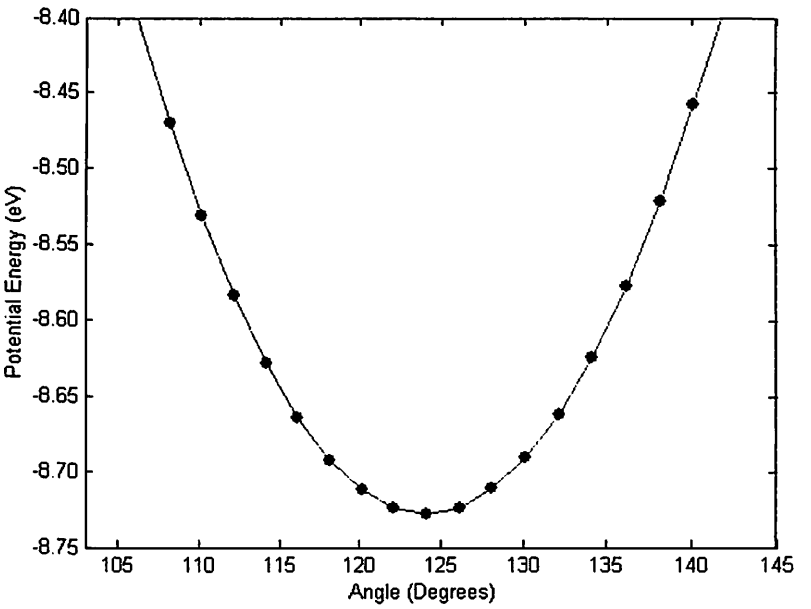

Figure 2.7

Ab initio potential energy at different $C^{(1)}C^{(2)}H^{(3)}$ angles

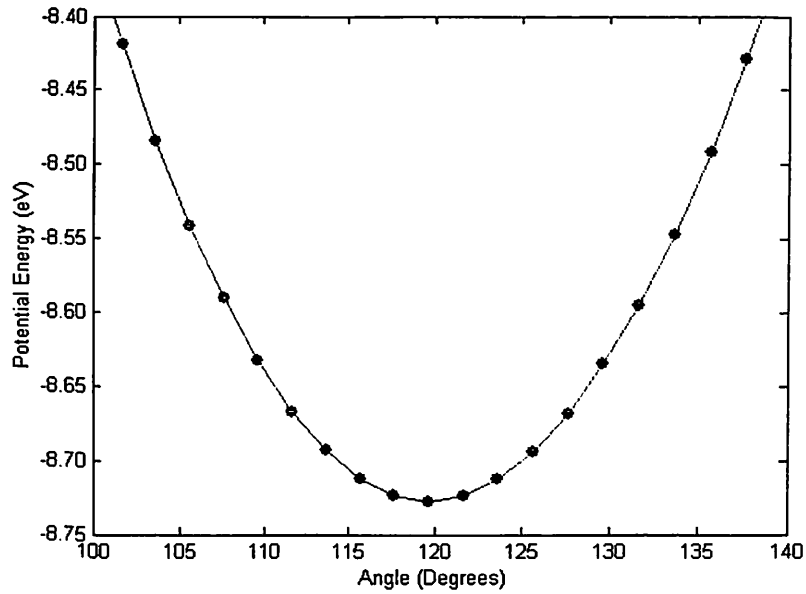

Figure 2.8

Ab initio potential energy at different $C^{(2)}C^{(1)}H^{(4)}$ angles

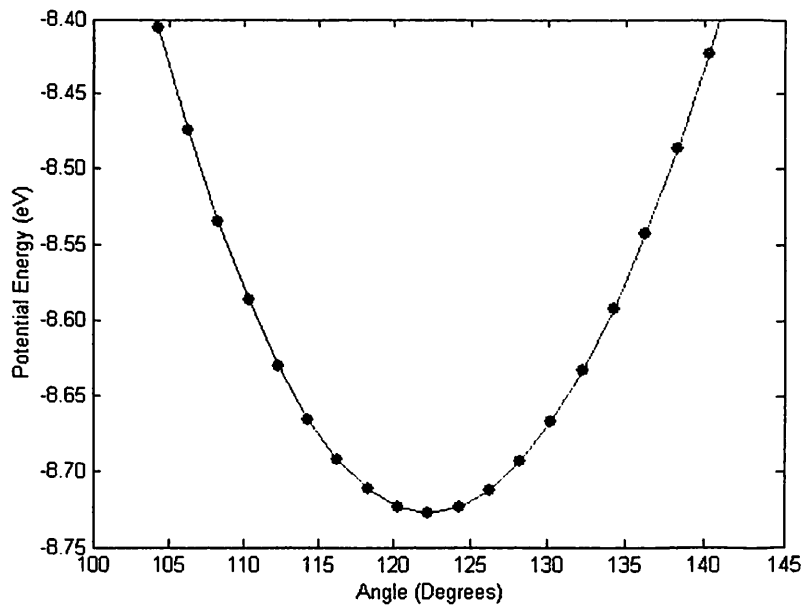

Figure 2.9

Ab initio potential energy at different $C^{(2)}C^{(1)}H^{(5)}$ angles

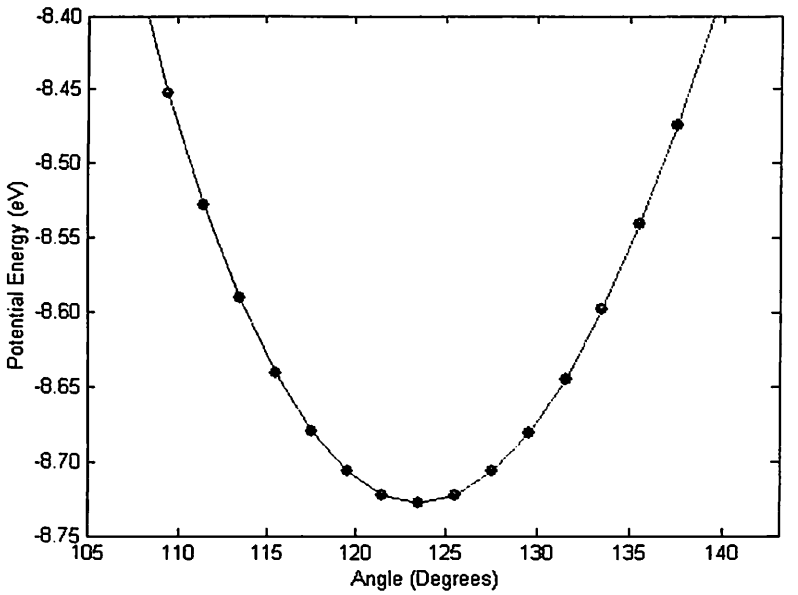

Figure 2.10

Ab initio potential energy at different $C^{(1)}C^{(2)}Br^{(6)}$ angles

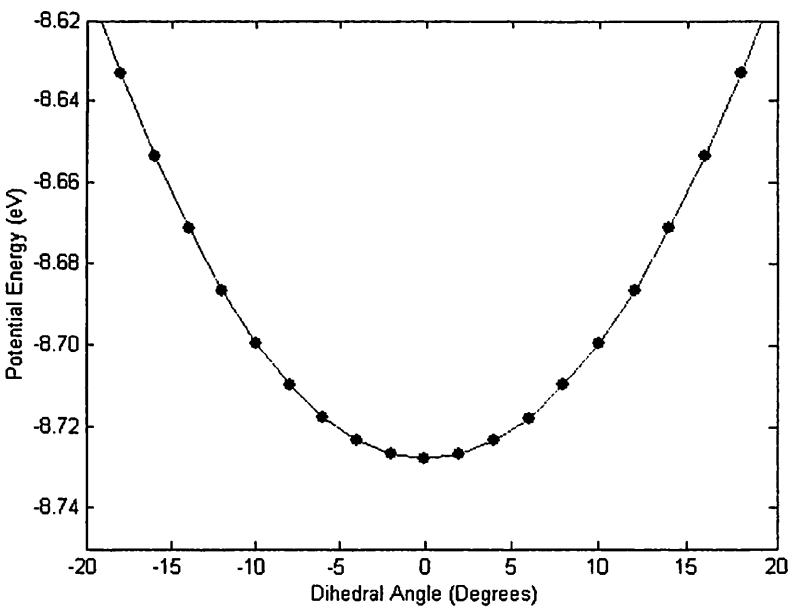

Figure 2.11

Ab initio potential energy at different $H^{(4)}H^{(3)}$ dihedral angles

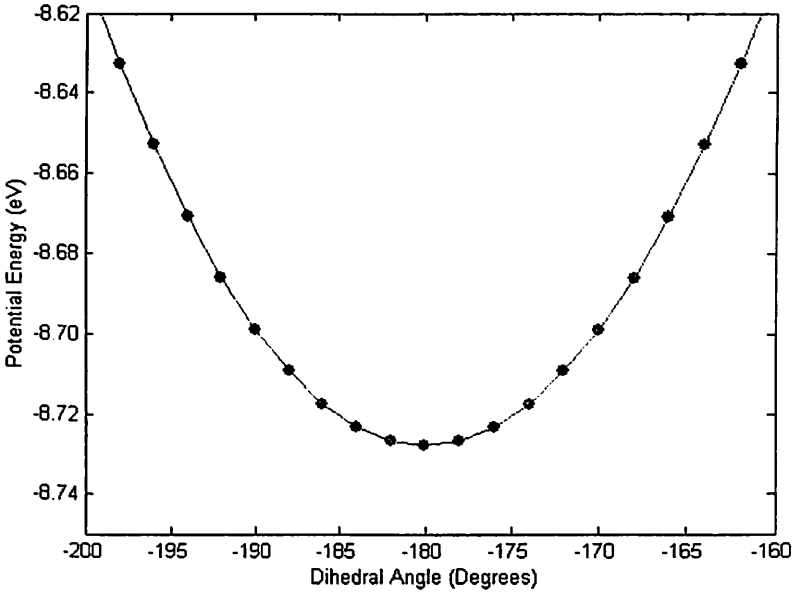

Figure 2.12

Ab initio potential energy at different $H^{(5)}H^{(3)}$ dihedral angles

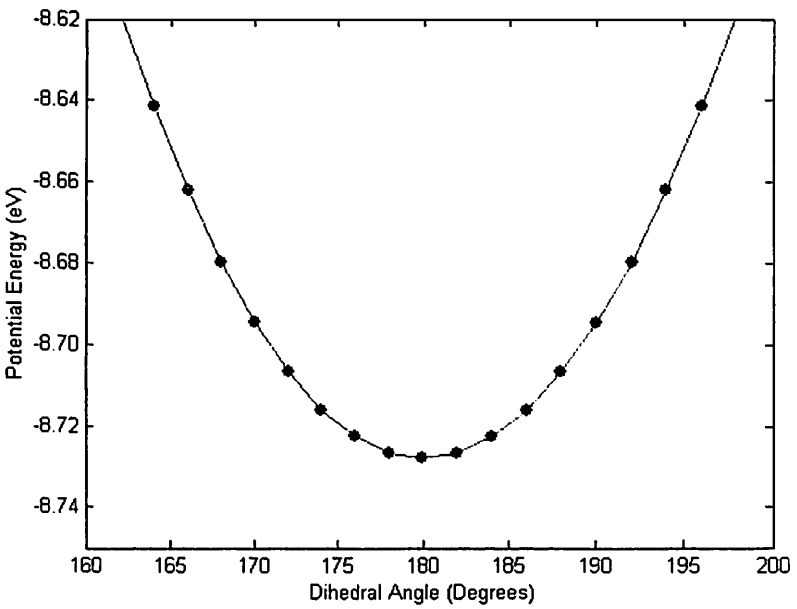

Figure 2.13

Ab initio potential energy at different $H^{(4)}Br^{(6)}$ dihedral angles

The technique we have just described served as a starting point, but the twelve-coordinate space we are using (five bond distances, four angles and three dihedral angles) is too large to be described fully. We need a sampling method to selectively represent the important regions of the hyperspace, and decided to make use of a molecular dynamics code originally developed by Rahaman and Raff[3] to accomplish this objective.

B. Sampling Methods

In order for us to sample the vast hyperspace with twelve coordinates, we needed to restrict the space by making use of the laws of chemistry and physics that govern molecular dynamics.

For this reason, we made use of a FORTRAN molecular dynamics code originally developed by Rahaman and Raff[3]. The code provided us with a means to check the different reaction pathways of the dissociation of vibrationally excited vinyl bromide and to identify the important channels. The code simulates what would happen to the vinyl bromide molecule if 6.44 eV were added to the system and randomly distributed among the twelve different vibrational modes of the molecule. We modified the code in such a way to have it stop 200 times, with equal time intervals in between the stops, and provide us with 200 different molecular configurations for every reaction pathway.

Now that the hyperspace was sampled by selecting the most prominent reaction pathways, we needed to calculate the potential for the different configurations we obtained from the molecular dynamics code. This meant that we would use the results from the molecular dynamics code as input parameters for GAUSSIAN 98W[1].

We calculated 600 molecular configurations using the potential scanning method described in Section II.A and 800 additional configurations using the molecular dynamics code method described in II.B.

With the 1,400 configurations calculated, we fitted the configurations using a neural network and thereby developed a PES for the dissociation of vibrationally-excited vinyl bromide.

An example of one configuration obtained from the molecular dynamics calculations and the *ab initio* potential energy calculated in GAUSSIAN 98W[1] leading to a 3-center elimination of HBr is shown in Table 2.14.

Table 2.14

Molecular dynamics code results and *ab initio* potential energy

Center	Cartesian Coordinates			*Ab initio* potential energy
	x	y	z	(Hartrees)
$C^{(1)}$	+1.20247	–0.00914	–1.96785	-2647.87278
$C^{(2)}$	+1.19247	+0.01682	–0.64294	
$H^{(3)}$	+1.94066	+0.11671	+0.08637	
$H^{(4)}$	+2.10691	–0.20750	–2.50298	
$H^{(5)}$	+0.53499	+0.09784	–2.72117	
$Br^{(6)}$	–0.41784	–0.00124	+0.45716	

As mentioned previously in Chapter I, Rahaman and Raff[3,4] did fit the PES but it took them over 9 months to complete the process, which is why we needed to fit the potential in a more accurate, less time consuming manner. The system we chose to

employ in order to accomplish this objective was the use of a self-adaptive, well-trained neural network.

C. Neural Network Fitting

In order to fit the PES, we chose to use neural networks for the following important reasons:

- Neural networks are robust when used with many parameters
- Neural networks use self-adaptive algorithms to fit themselves to a set of predetermined input and output parameters
- Neural networks are excellent with interpolations where the set of values to be predicted lie within a well-defined hyperspace region
- Neural networks employ parallel organization, which permits them to find solutions to problems where multiple constraints must be satisfied simultaneously

The last of the four reasons is crucial in our case because more than one parameter can affect the potential simultaneously, which in our case translates to a contribution to the potential from bond distances, angles, dihedral angels or any combination of them as well.

Before we see how neural networks were used to fit the PES, let us have a look at the architecture of neural networks.

Neural networks are logical entities that accept inputs, produce outputs and are made up of neurons and transfer functions. An elementary neuron accepts a set of inputs

"P_T" and multiplies them by a set of weights "W_T". Each input "p_i" is multiplied by a given weight "w_i" and added to a bias "b". The sum of the weighted inputs and the bias forms the input to the transfer function "f". Neurons may use any differentiable transfer function "f" to generate their output.[5] A general neuron is shown in Figure 2.14.

One type of transfer function is the sigmoid function. This function produces output values that are always in the range –1 to +1. We used the "TANSIG" sigmoid transfer function, which is given by the following equation:

$$\text{TANSIG}(n) = \frac{2}{1 + e^{-2n}} - 1 \qquad \text{where } n = \Sigma (p_i * w_i + b)$$

TANSIG takes a matrix of net input vectors and returns a value for each element of the input vectors between –1 and +1.

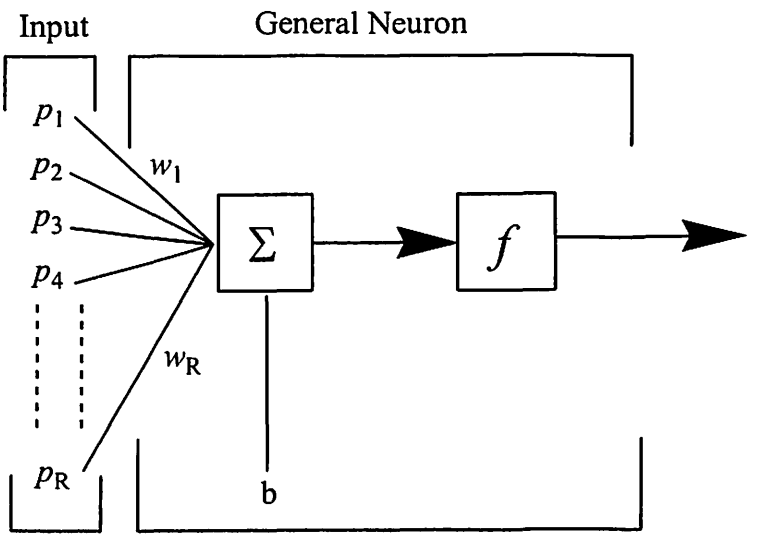

Figure 2.14

A general neuron

A special type of neural networks is the feedforward neural network that often has one or more hidden layers of neurons being transferred by sigmoid functions followed by an output layer produced by a linear function.

Multiple layers of neurons with nonlinear transfer functions allow the network to learn nonlinear and linear relationships between input and output vectors. The linear function generating the output layer lets the network produce values outside the range –1 to +1.[6] A typical feedforward network is shown in Figure 2.15.

Neural networks are adjusted or trained so that a particular input leads to a specific target output. The network is trained based on a comparison of the output and the target until the network output matches the target. Typically many input and target pairs are used in training a neural network. This process is referred to as supervised neural network training or learning.[6]

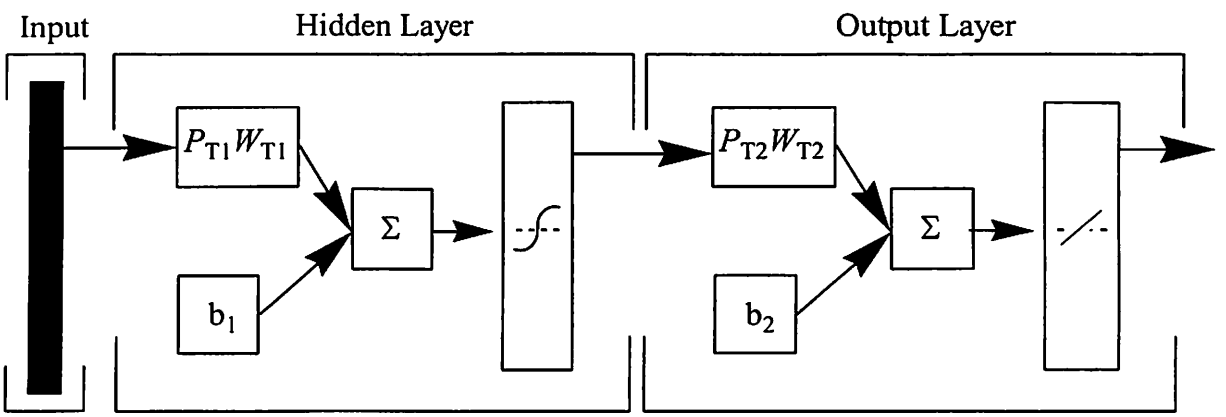

Figure 2.15

A typical feedforward neural network

Once the neural network is trained, it can be used to predict the output value for an input it was not trained with. The neural network can interpolate well whereas it

extrapolates poorly.[5] This means that the prediction a neural network makes for a certain input is only valid if the input lies within a region of the hyperspace in which the neural network is well trained. The result of a well-trained neural network is a smoothly fitted hypersurface.

References:

1. M. J. Frisch, G. W. Trucks, H. B. Schlegel, P. M. W. Gill, B. G. Johnson, M. A. Robb, J. R. Cheeseman, T. Keith, G. A. Peterson, J. A. Montgomery, K. Raghavarachi, M. A. Al-Laham, V. G. Zakrzewski, J. V. Ortiz, J. B. Foresman, J. Cioslowski, B. B. Stefanov, A. Nanayakkara, M. Challacombe, C. Y. Peng, P. Y. Ayala, W. Chen, M. W. Wong, J. L. Andres, E. S. Replogle, R. Gomperts, R. L. Martin, D. J. Fox, J. S. Binkley, D. J. Defrees, J. Baker, J. P. Stewart, M. Head-Gordon, C. Gonzales and J. A. Pople, *Gaussian 98W Revision A.7*, Gaussian Inc., Pittsburgh PA (1999).

2. S. Huzinaga J. Andselm, M Klobukowski, E. Radzio-Andzelm, Y. Sakai and H. Tatewaki, *Gaussian Basis Sets for Molecular Calculations*, Elsevier, Amsterdam, Oxford, New York, Tokyo (1984).

3. A. Rahaman Ph. D. Dissertation, Oklahoma State University at Stillwater (2000).

4. A. Rahaman and L. M. Raff, *J. Phys. Chem. A* **105**, 2156 (2001).

5. M. T. Hagan, H. B. Demuth and M. Beale, *Neural Network Design*, PWS Publishing, Boston MA (1996).

6. Martin Anthony and Peter L. Bartlett, *Neural Network Learning: Theoretical Foundations*, Cambridge University Press, New York City NY (1999).

CHAPTER III

APPLICATION TO THE VINYL BROMIDE SYSTEM

As mentioned previously in Section I., we chose vinyl bromide as our system because its size is adequate for computational purposes, it is not too small yet not too big, and it has been well studied experimentally making it easy for us to carefully evaluate the accuracy of our results. In addition, there are six energetically open reaction channels all of which must be accurately described to properly investigate the reaction dynamics. As described in Section II.A, the potential energy was calculated for 600 molecular configurations using GAUSSIAN 98W[1] by either stretching a bond distance or bending an angle or a dihedral angle of vinyl bromide.

We fitted the 600 potentials we calculated with a 20-neuron, 2-layer MATLAB R12[2] neural network that we trained using the Levenberg-Marquardt algorithm[2] and compared the neural network results with those of GAUSSIAN 98W[1]. We chose to use a TANSIG function as our transfer function, which is why we used the scaling formula described in Section II.A. The scaling function ensured that the relative potential-energy values would fall in the range –1 to +1, which matches perfectly with the range of a TANSIG function and produces a better fit. Once we obtained the scaled results, we converted them back to their original values using the function:

$$K = K_{\min} + (K_{\mathrm{Rel}} + 1)(K_{\max} - K_{\min}) / 2$$

We found the original potential-energy values, converted the units from "Hartree" to "eV" and plotted the results. The results are shown in Figures 3.1 though 3.12.

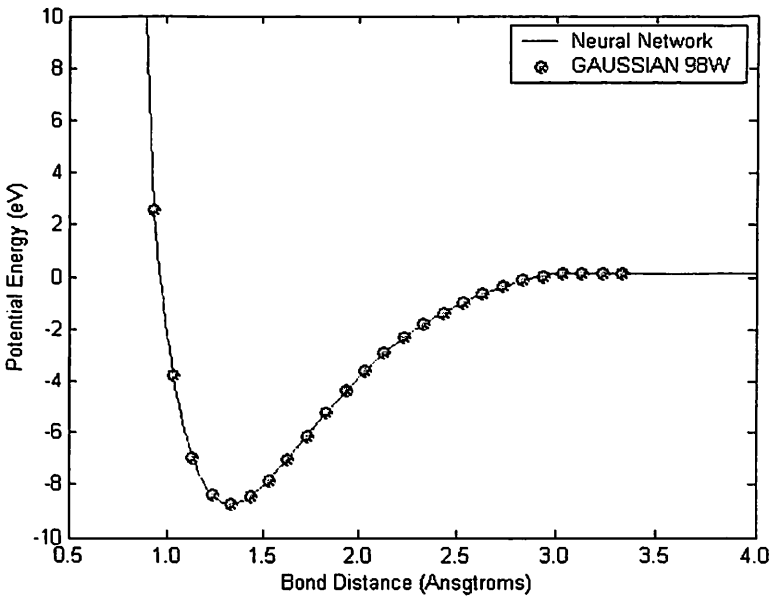

Figure 3.1

Neural network and *ab initio* results at different $C^{(1)}$=$C^{(2)}$ bond distances

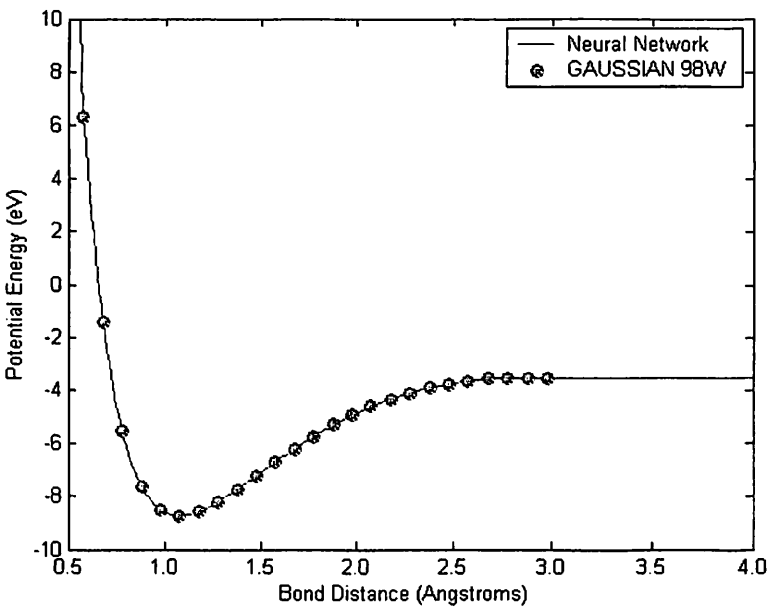

Figure 3.2

Neural network and *ab initio* results at different $C^{(2)}$-$H^{(3)}$ bond distances

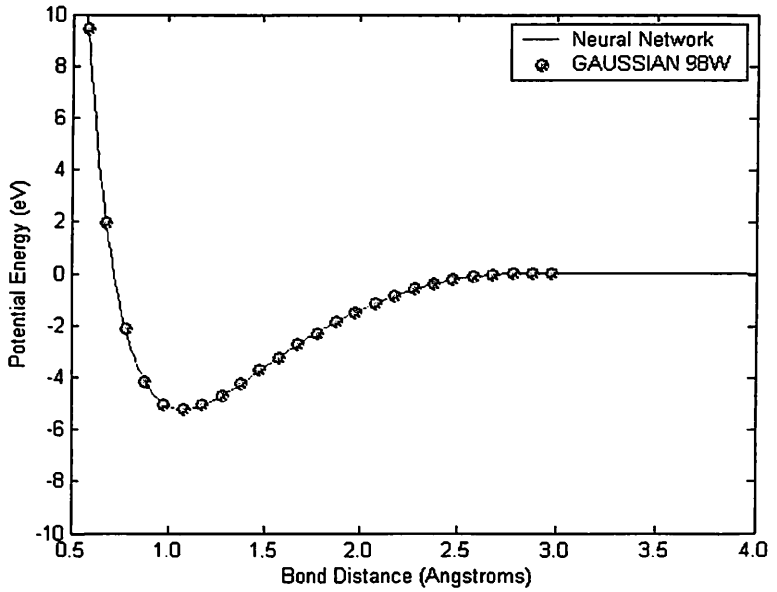

Figure 3.3

Neural network and *ab initio* results at different $C^{(1)}$-$H^{(4)}$ bond distances

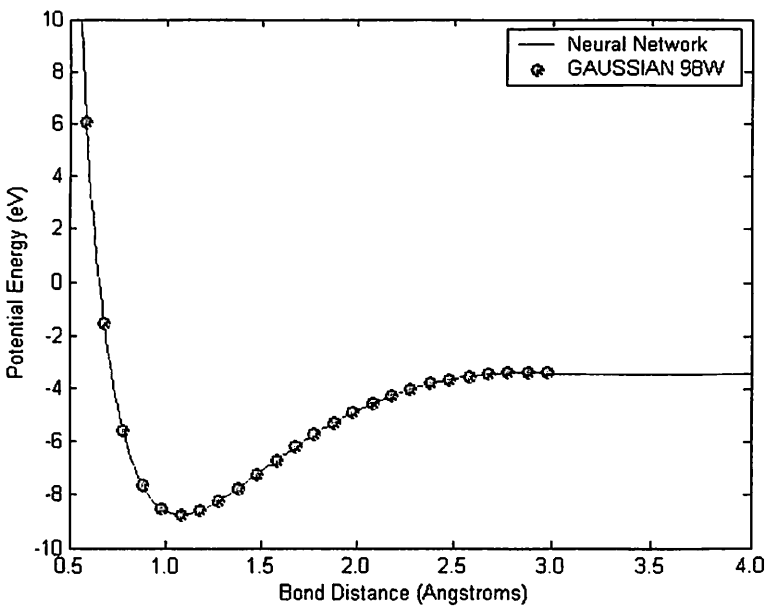

Figure 3.4

Neural network and *ab initio* results at different $C^{(1)}$-$H^{(5)}$ bond distances

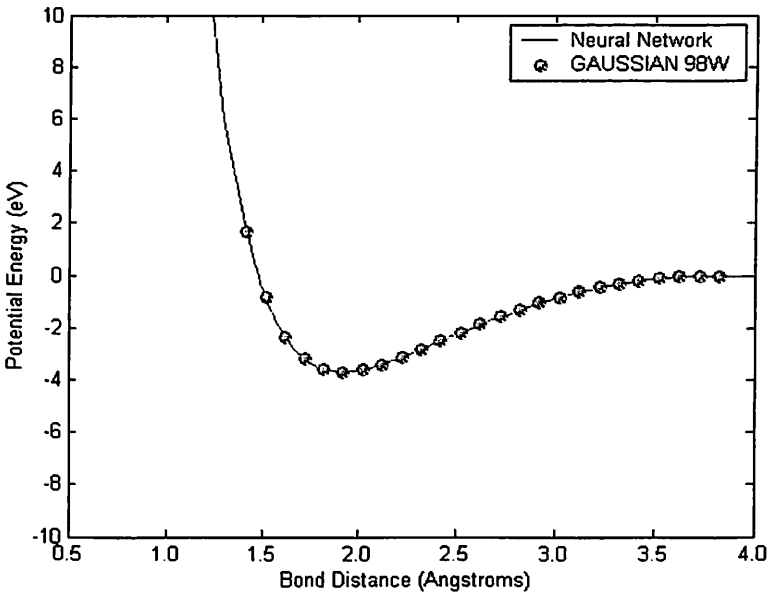

Figure 3.5

Neural network and *ab initio* results at different $C^{(2)}$-$Br^{(6)}$ bond distances

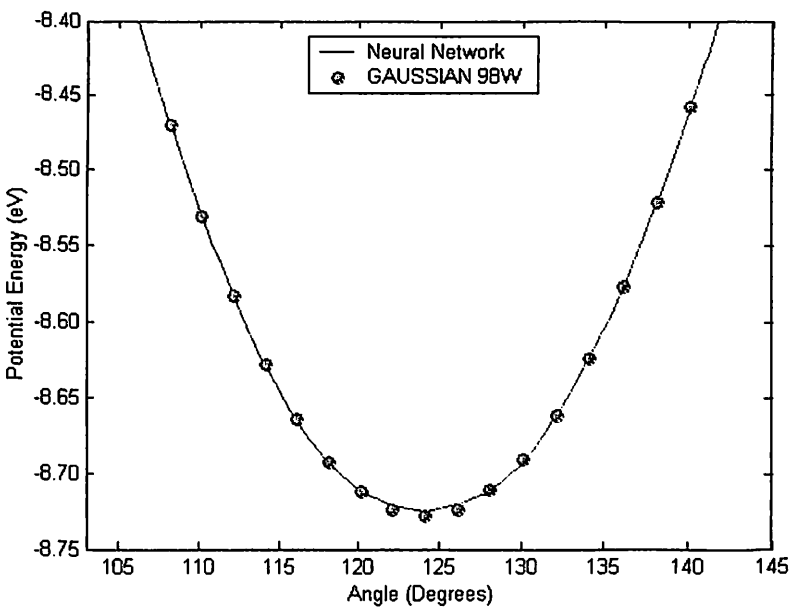

Figure 3.6

Neural network and *ab initio* results at different $C^{(1)}C^{(2)}H^{(3)}$ angles

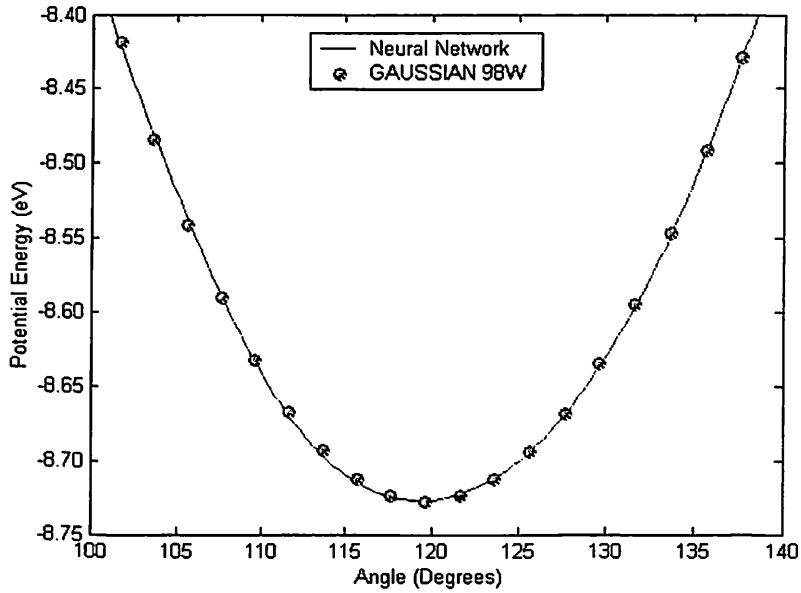

Figure 3.7

Neural network and *ab initio* results at different $C^{(2)}C^{(1)}H^{(4)}$ angles

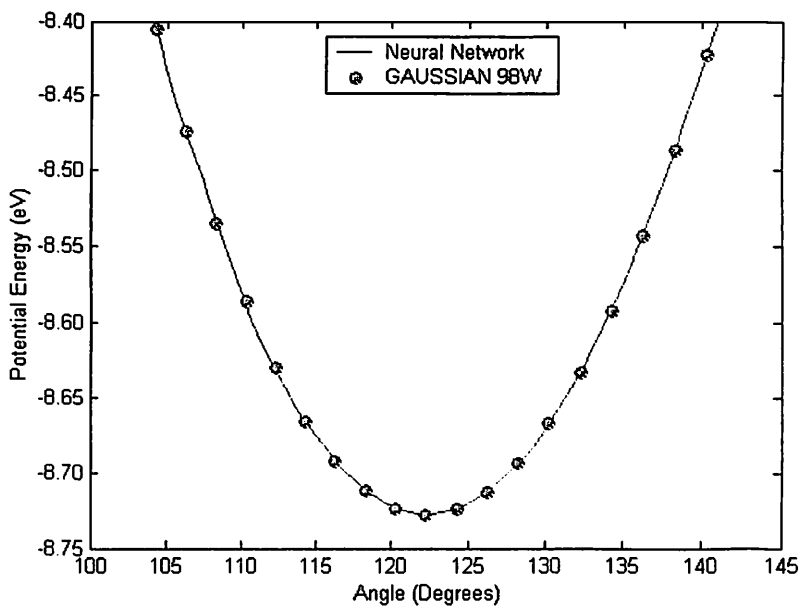

Figure 3.8

Neural network and *ab initio* results at different $C^{(2)}C^{(1)}H^{(5)}$ angles

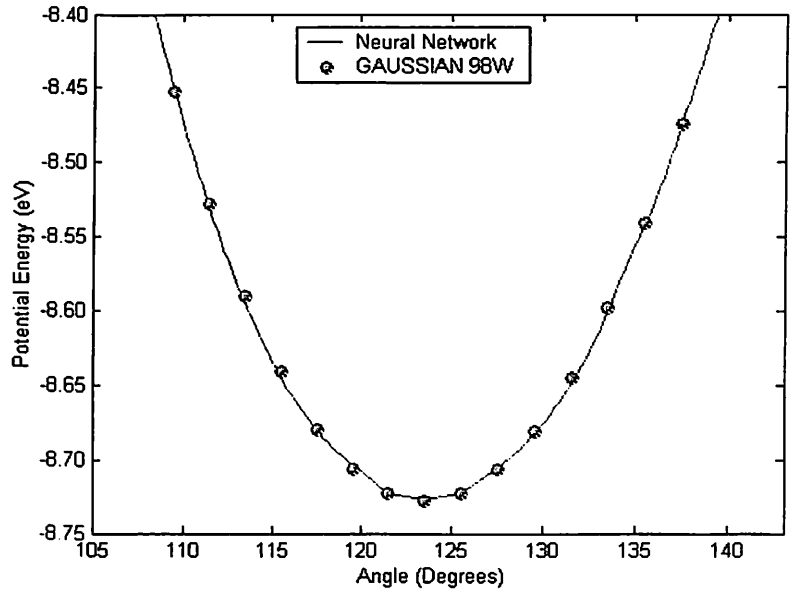

Figure 3.9

Neural network and *ab initio* results at different $C^{(1)}C^{(2)}Br^{(6)}$ angles

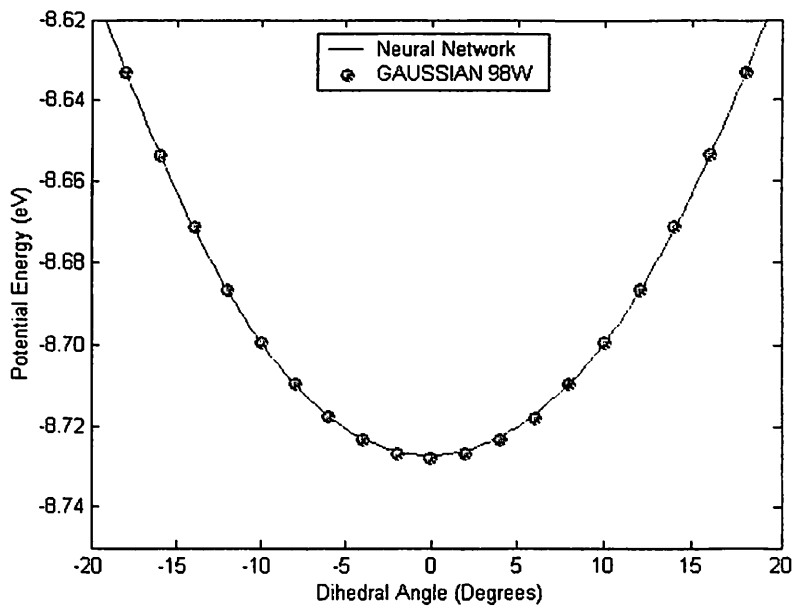

Figure 3.10

Neural network and *ab initio* results at different $H^{(4)}H^{(3)}$ dihedral angles

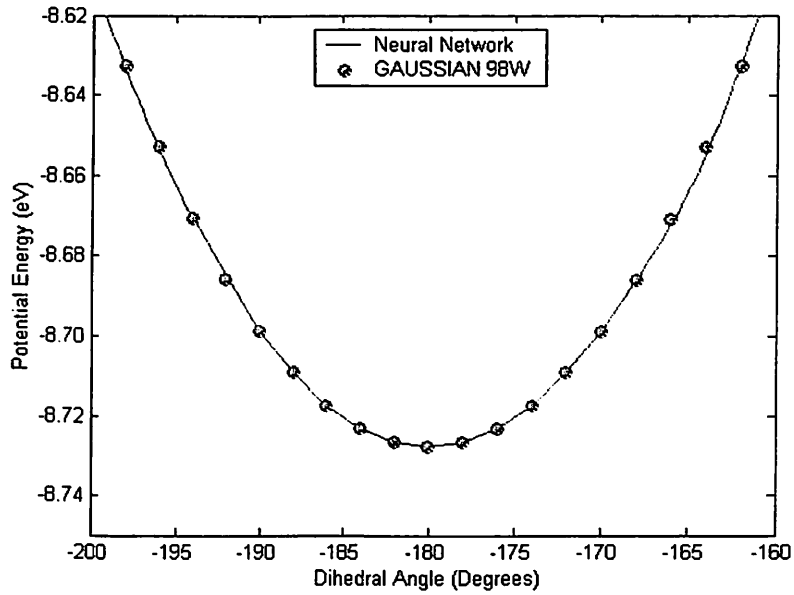

Figure 3.11

Neural network and *ab initio* results at different $H^{(5)}H^{(3)}$ dihedral angles

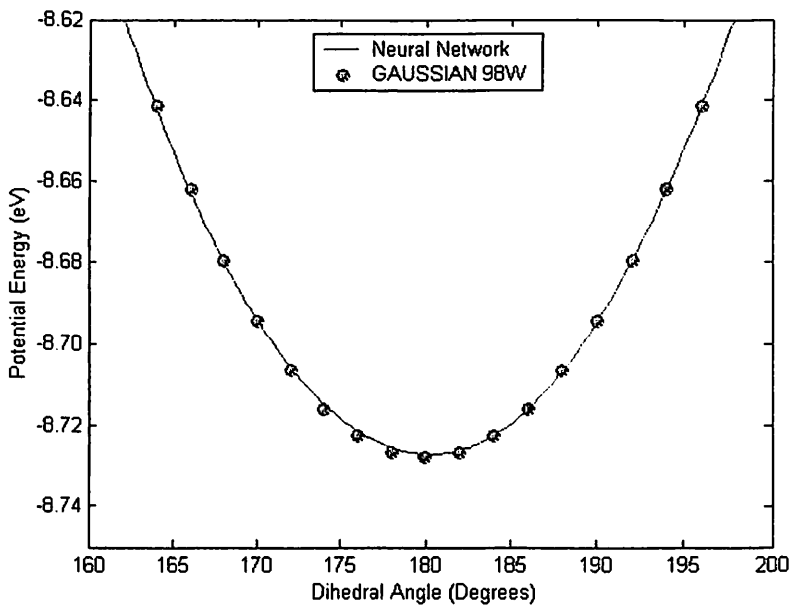

Figure 3.12

Neural network and *ab initio* results at different $H^{(4)}Br^{(6)}$ dihedral angles

As described in Section II.B, another 800 potential energies were derived from using the molecular dynamics code, written by Rahaman and Raff[3], to get molecular configurations that would serve as input parameters for GAUSSIAN 98W[1].

We fitted the 1,400 potentials we calculated with a MATLAB R12[2] neural network, into a potential surface and developed a PES for the dissociation of vibrationally excited vinyl bromide. The fitting process took approximately 6 minutes.

To compare the PES we developed using MATLAB R12[2] with that obtained from the *ab initio* calculations we plotted the scaled results from the neural network versus those from GAUSSIAN 98W[1]. The results are shown in Figure 3.13.

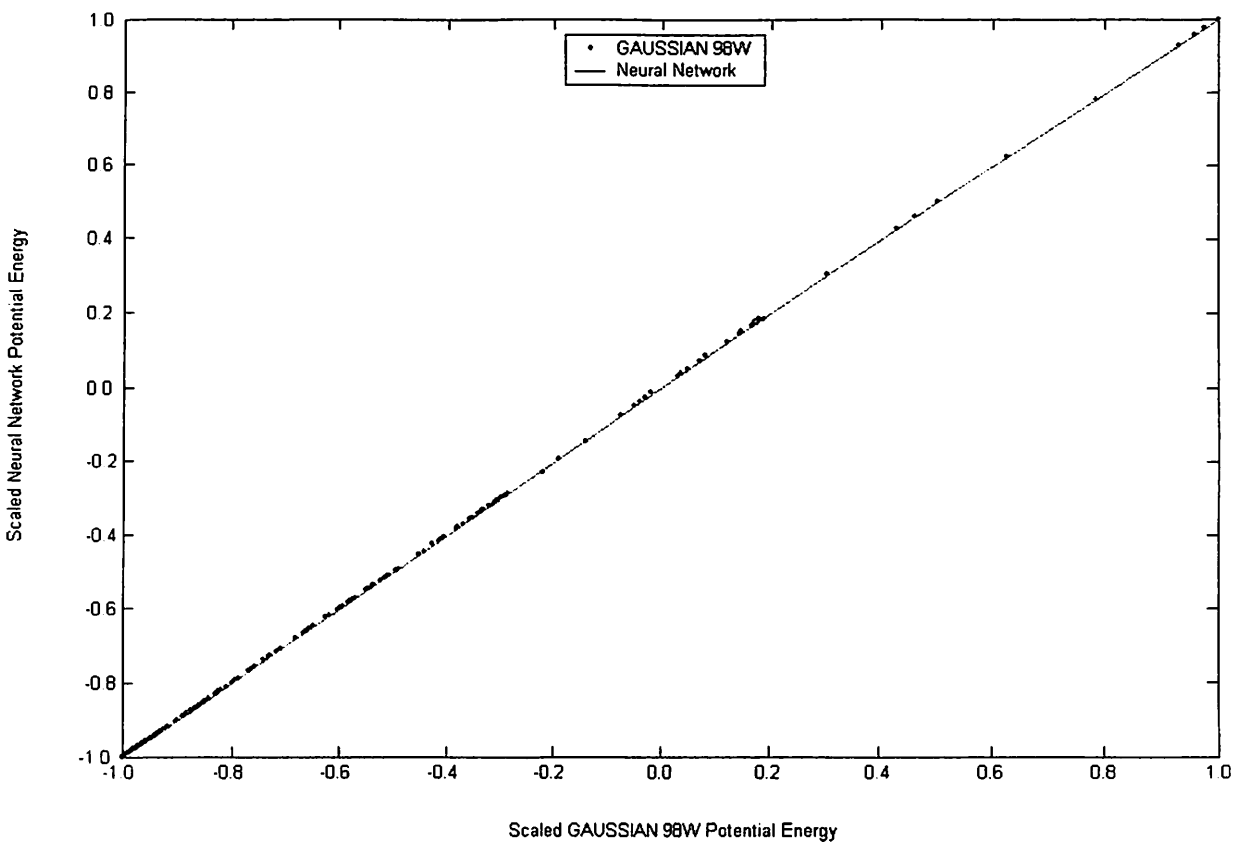

Figure 3.13

Neural network vs. *ab initio* results

The standard deviation of the results from the neural network and those from the *ab initio* calculations is 9.5078×10^{-4} suggesting that the fit was near identical and the results were highly accurate.

Figure 3.14 is another representation of the results from the neural network and those from the *ab initio* calculations. It is a distribution histogram of the deviation between the *ab initio* calculations and the neural network results. In Figure 3.14, the points are the results obtained from the neural network and the *ab initio* calculations. The smooth curve is a least-squares fit of the Lorentzian function given by the equation:

$$y = \frac{\alpha}{(x - \beta)^2 + \sigma^2}$$

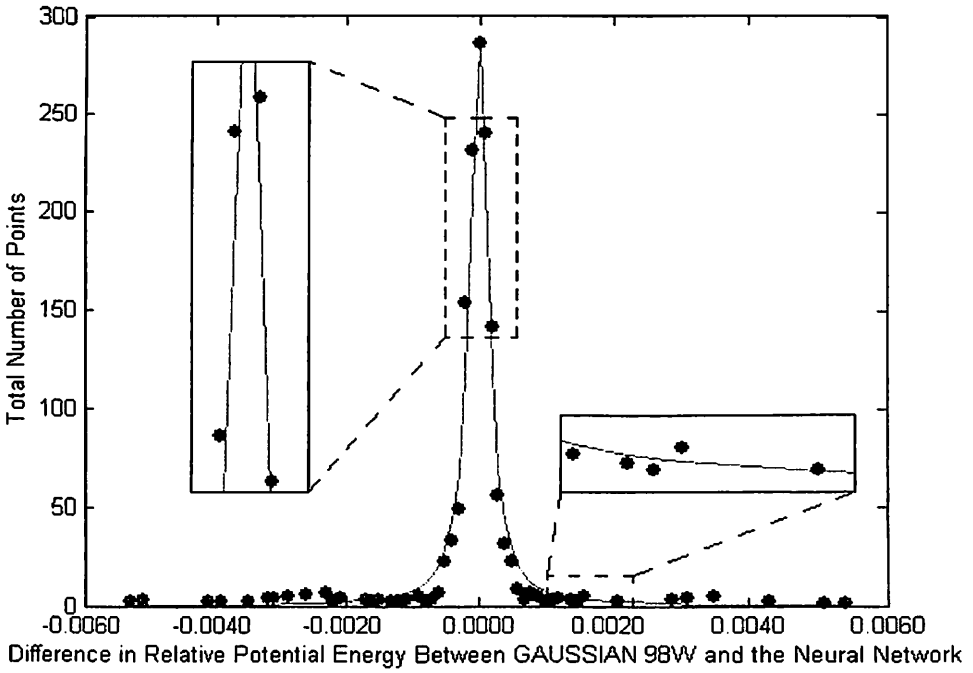

Figure 3.14

Ab initio and neural network deviation distribution

The respective values for α, β and σ of the Lorentzian fitting function in Figure 3.14 are 8.01×10^{-6}, 1.43×10^{-6} and 1.67×10^{-4}. The small size of β indicates that the results from the neural network are highly comparable to the ones from the *ab initio* calculations.

References:

1. M. J. Frisch, G. W. Trucks, H. B. Schlegel, P. M. W. Gill, B. G. Johnson, M. A. Robb, J. R. Cheeseman, T. Keith, G. A. Peterson, J. A. Montgomery, K. Raghavarachi, M. A. Al-Laham, V. G. Zakrzewski, J. V. Ortiz, J. B. Foresman, J. Cioslowski, B. B. Stefanov, A. Nanayakkara, M. Challacombe, C. Y. Peng, P. Y. Ayala, W. Chen, M. W. Wong, J. L. Andres, E. S. Replogle, R. Gomperts, R. L. Martin, D. J. Fox, J. S. Binkley, D. J. Defrees, J. Baker, J. P. Stewart, M. Head-Gordon, C. Gonzales and J. A. Pople, *Gaussian 98W Revision A.7*, Gaussian Inc., Pittsburgh PA (1999).

2. *Matlab R12*, The MathWorks Inc., Boston MA (2001).

3. A. Rahaman Ph. D. Dissertation, Oklahoma State University at Stillwater (2000).

CHAPTER IV

CONCLUSIONS AND FUTURE WORK

Our work has shown that using neural networks to fit potential energies and generate a potential-energy surface yields results that are very close in accuracy to those generated using *ab initio* calculations.

The main advantage of using neural networks resides in the fact that it takes the neural network a very small fraction of the time it takes a human being to generate a same or similar potential-energy surface. While it took Rahaman and Raff[1,2] over 9 months to generate and fit the PES, it took us less than a month to reach the same goal using a feedforward neural network with a sigmoid transfer function.

The standard deviation of 9.5078×10^{-4} is a good indication of how close the MATLAB R12[3] neural network results are from those of the *ab initio* calculations using GAUSSIAN 98W[4].

Future work in this project might include using the neural network as input for the molecular dynamics code without having to go through the tedious algebraic work that Rahaman and Raff[1,2] had to go through to fit their potential-energy surface.

Another project might include using neural networks to fit the forces on each atom in vinyl bromide into a force hypersurface then differentiating our potential-energy surface to get a force hypersurface and comparing the two force hypersurfaces.

A third project might include using neural networks to fit the forces on each atom in vinyl bromide into a force hypersurface then integrating the force hypersurface and getting a potential-energy surface the results of which we could compare to the ones we generated in our investigation.

References:

1. A. Rahaman Ph. D. Dissertation, Oklahoma State University at Stillwater (2000).

2. A. Rahaman and L. M. Raff, *J. Phys. Chem. A* **105**, 2156 (2001).

3. *Matlab R12*, The MathWorks Inc., Boston MA (2001).

4. M. J. Frisch, G. W. Trucks, H. B. Schlegel, P. M. W. Gill, B. G. Johnson, M. A. Robb, J. R. Cheeseman, T. Keith, G. A. Peterson, J. A. Montgomery, K. Raghavarachi, M. A. Al-Laham, V. G. Zakrzewski, J. V. Ortiz, J. B. Foresman, J. Cioslowski, B. B. Stefanov, A. Nanayakkara, M. Challacombe, C. Y. Peng, P. Y. Ayala, W. Chen, M. W. Wong, J. L. Andres, E. S. Replogle, R. Gomperts, R. L. Martin, D. J. Fox, J. S. Binkley, D. J. Defrees, J. Baker, J. P. Stewart, M. Head-Gordon, C. Gonzales and J. A. Pople, *Gaussian 98W Revision A.7*, Gaussian Inc., Pittsburgh PA (1999).

VITA

Dany Doughan

Candidate for the Degree of

Master of Science

Thesis: NEURAL NETWORKS AS A MEANS TO FIT THE POTENTIAL ENERGY SURFACE OF VINYL BROMIDE

Major Field: Chemistry

Biographical:

Education: Graduated from the International College, Beirut, Lebanon in June 1994, received Bachelor of Science Degree in Chemistry from the Lebanese American University, Beirut, Lebanon in June 1998. Completed the requirements for a Master of Science with a major in Computer Science at the Lebanese American University, Beirut, Lebanon, Department of Natural Sciences in December 2001. Completed the requirements for a Master of Science with a major in Physical Chemistry at Oklahoma State University, Department of Chemistry in May 2004.

Experience: Teaching assistant at the Lebanese American University, Beirut Lebanon, August 1998 to December 2000; Teaching Assistant at Oklahoma State University, January 2001 to May 2004.

Professional Memberships: Phi Lambda Upsilon
American Chemical Society